JMEPEG (2024) 33:8994–9003
https://doi.org/10.1007/s11665-023-08894-2

1059-9495/$19.00

ORIGINAL RESEARCH ARTICLE

Microstructural and Mechanical Properties of Cr-Ni_3Al Alloy Films Synthesized by Magnetron Sputtering

Sunil Kumar Tiwari, Akula Umamaheswara Rao, Archana Singh Kharb, Vipin Chawla, Jitendra Kumar Pandey, Vikas Saxena, Neha Sardana, Devesh Kumar Avasthi, and Amit Kumar Chawla

Submitted: 29 May 2023 / Revised: 24 September 2023 / Accepted: 9 October 2023 / Published online: 10 November 2023

Cr-Ni_3Al alloy films have been deposited on Si (100) substrate via DC magnetron sputtering. The effect of Cr enrichment on microstructure and mechanical properties has been studied. The evolution of phases, microstructure, surface topography and mechanical properties has been studied using GI-XRD, FE-SEM, AFM and quasi-static nanoindentation, respectively. Results revealed that the alloy films possessed a preferred orientation of (111) plane with a maximum hardness and Young's modulus of ~ 12.7 GPa and ~ 203 GPa for 0 W Cr-Ni_3Al films which further decreased to ~ 7 GPa and 129 GPa, respectively, for 40 W Cr-Ni_3Al films. The reported values of hardness and Young's modulus are very high in the case of alloy Ni_3Al-based coatings when compared with the literature. This study also imitates that with the increase in Cr concentration in the host Ni_3Al matrix, the surface roughness increased as a result of the evolution of pores. However, hydrophobicity is observed to be increased with increase in Cr concentration in host Ni_3Al coatings with a maximum contact angle of 115.9° for 40 W Cr-Ni_3Al alloy film.

Keywords FE-SEM, hardness, hydrophobic property, magnetron sputtering, microstructure, Ni_3Al

1. Introduction

Over the past two decades, transition metal-based thin films are synthesized and characterized by several researchers for high-temperature applications (Ref 1, 2). These coatings have shown excellent mechanical and tribological properties at ambient and elevated temperatures (Ref 3-5). Moreover, some of the transition metal nitride coatings such as CrN, TiN, WN, etc., and Ni- and Ti-based coatings have shown enhanced properties in terms of corrosion and oxidation resistance along with microstructural stability (Ref 6-8). Looking into the demand for high-temperature structural applications, researchers have fabricated, nickel and nickel superalloy-based coating because of their high thermal stability (Ref 9, 10). In the past decade, the demand for enhanced surface properties and strength such as hardness and wear resistance in semiconductor, microelectronics and machining industries has led to the development of coatings with enhanced mechanical and tribological properties along with high-temperature stability (Ref 9-11). In particular, Ni_3Al-based intermetallic compound coatings with excellent properties such as creep and fatigue resistance, thermal stability, high stiffness and high melting point make them a potential candidate for high-temperature applications such as gas turbine blades, jet engines, aerospace and nuclear industries (Ref 12-17). Moreover, doping of transition metals such as W, Cr, Pd and B in Ni_3Al films in alloy or multilayer forms also alters their properties and mechanical behavior at ambient and high temperature (Ref 18-20). Alloying Ni_3Al intermetallic with Fe has increased mechanical properties whereas it has resulted in improving high-temperature strength when doped with zirconium (Zr) because of solid solution hardening (Ref 21). It has been reported that boron doped in Ni_3Al films, extensively occupies the Al sites, or the element which is a substitute for both Al and Ni is ductilized by boron resulting in increasing the overall ductility of the film (Ref 22). While synthesizing Ni_3Al-based coatings, phase formation and microstructure have a great impact on mechanical and tribological properties. It has been reported that with an increase in crystallite size, the hardness generally decreases and vice versa following the Hall–Petch,

Sunil Kumar Tiwari, Department of Mechanical Engineering, SoE, University of Petroleum and Energy Studies, Energy Acres, Bidholi, Dehradun, Uttarakhand 248007, India; and School of Technology, Woxsen University, Hyderabad, Telangana 502345, India; **Akula Umamaheswara Rao** and **Vikas Saxena**, Department of Mechanical Engineering, SoE, University of Petroleum and Energy Studies, Energy Acres, Bidholi, Dehradun, Uttarakhand 248007, India; **Archana Singh Kharb** and **Amit Kumar Chawla**, Department of Physics, Applied Science Cluster, SoE, University of Petroleum and Energy Studies, Energy Acres, Bidholi, Dehradun, Uttarakhand 248007, India; **Vipin Chawla**, Institute Instrumentation Center, IIT Roorkee, Roorkee, Uttarakhand 247667, India; **Jitendra Kumar Pandey**, University of Petroleum and Energy Studies, Energy Acres, Bidholi, Dehradun, Uttarakhand 248007, India; **Neha Sardana**, Department of Materials and Metallurgical Engineering, Indian Institute of Technology, Ropar, Roopnagar, Punjab 140001, India; and **Devesh Kumar Avasthi**, Department of Physics, Applied Science Cluster, SoE, University of Petroleum and Energy Studies, Energy Acres, Bidholi, Dehradun, Uttarakhand 248007, India; and Center for Interdisciplinary Research and Innovation, University of Petroleum and Energy Studies, Energy Acres, Bidholi, Dehradun, Uttarakhand 248007, India. Contact e-mail: amit.phy@gmail.com.

Graphical Abstract

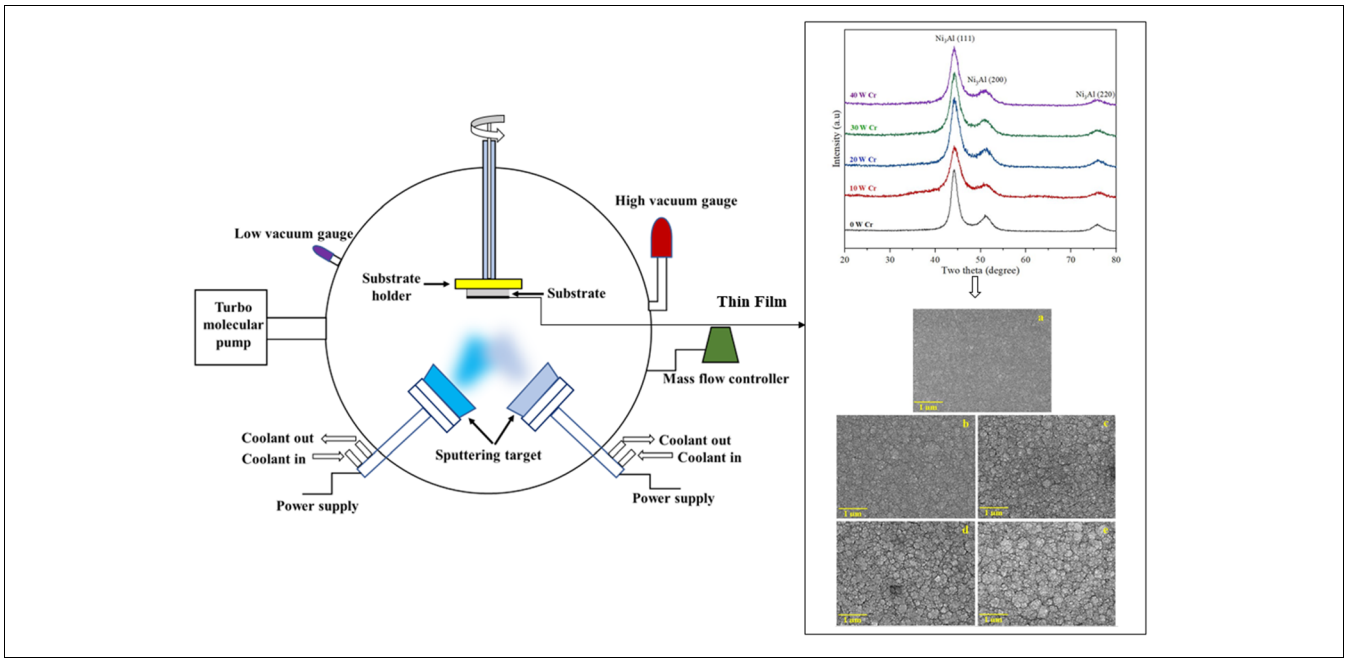

but in some cases, inverse Hall–Petch results have been observed (Ref 19, 23, 24). In the literature, it has been found that, despite increasing the crystallite and grain size of the film, mechanical and tribological properties have increased. This has been perceived because of the formation of ordered $L1_2$ preferred orientation of Ni_3Al films which contributes to increasing the hardness of the film (Ref 25).

There are several factors affecting the properties and microstructure of Ni_3Al films while depositing via magnetron sputtering. Sputtering process parameters such as sputtering pressure and substrate temperature influence grain growth, refinement and rearrangement which results in altering the properties of the film (Ref 26). Moreover, heat treatment post-deposition also contributes to varying the properties of the Ni_3Al films.

Swygenhoven et al. (Ref 27) deposited Ni_3Al alloy and Ni/Ni_3Al multilayer films on Si substrate via DC magnetron sputtering. To study the hardness of the film, alloy Ni_3Al film was deposited with 400-nm thickness whereas the multilayer films were deposited with two different layer thicknesses of Ni_3Al/Ni as 2.5 nm and 5 nm. Researchers found that the alloy films showed a maximum hardness of $\sim$ 13 GPa whereas the Ni/Ni_3Al with an individual layer thickness of 5 nm showed a hardness of $\sim$ 12 GPa, and the film with an individual layer thickness of 2.5 nm showed a hardness of 11.8 GPa. Thin films deposited in the form of alloy and multilayers have shown enhanced hardness as compared to that of the bulk Ni_3Al ($\sim$9.5 GPa).

Ng et al. (Ref 8) deposited Ni_3Al films onto the Ni substrate using the multitarget system by putting the Ni and Al sheets glued together on a thin circular metal sheet and with casted alloy Ni_3Al targets also via sputtering. They found that the sputtering yield of Ni was more as compared to Al. Accordingly, they claimed that to find the composition in the ratio of 75:25 at.% (Ni:Al), the multitarget should have an area of 23Ni:13Al whereas the alloy target should have the composition of Ni-32at.%Al. The results of microhardness revealed that the as-deposited film and the film annealed at 300 °C showed almost the same hardness whereas the maximum hardness was shown by the film annealed at 700 °C. They also found a continuous fall in hardness as a result of an increase in indentation depth.

Xing et al. (Ref 26) in their research to synthesize Ni_3Al and Ni_3Al/Cr multilayer films found that the hardness Ni_3Al Cr decreased as compared to single-layered Ni_3Al films whereas Young's modulus increased. They also found that both the single-layered and multilayered films were able to prevent the substrate from being drastically oxidized at an elevated temperature of 900 °C whereas the toughness of multilayer films was increased.

Zhang et al. (Ref 19) found that the hardness of Ni_3Al films doped with ultra-thin Cr layers in multilayer forms increased with an increase in Cr content and annealing temperature. In their further research while synthesizing Ni/Ni_3Al multilayer films, with different individual layer thicknesses of Ni and Ni_3Al (layer thickness $h < 100$ and $h = 160$), they found that the Ni/Ni_3Al film showed the preferred orientation of (111) texture. It is seen that with decreasing individual layer thickness, there appears a peak broadening in the XRD spectrum reflecting a decrease in the crystallite size of the film. Results of nanoindentation showed that the hardness of the annealed films was low as compared to as-deposited Ni/Ni_3Al films which further decreased with an increase in the individual layer thickness of Ni and Ni_3Al (Ref 23). In our previous research, alloy Ni_3Al films were deposited on Si substrate via DC magnetron sputtering (Ref 28). The result of nanoindentation revealed that the alloy Ni_3Al film possessed a hardness of $\sim$ 13 GPa as reported by Swygenhoven et al. (Ref 27) while enriching the film further with Ni via co-sputtering, it was observed that the hardness and Young's modulus of the film decreased with the evolution of cracks and pores.

Several research groups have studied the properties and behavior of Ni_3Al-based films at ambient and high temperatures. However, very limited research is available in the

literature in the case of alloy deposition particularly using dopants in alloy form. The present work reports on the effect of Cr in Ni_3Al films in alloy form on its microstructural and mechanical properties for their application in microelectronic devices, molding industries and structural application in aerospace industries.

2. Experimental Procedure

2.1 Synthesis of Film

Cr-Ni_3Al alloy films were deposited on Si (100) substrates via co-sputtering. The films were deposited at a substrate temperature of 400 °C in a custom-designed vacuum chamber. Alloy target of Ni_3Al (2-inch diameter and 5-mm thickness; 99.99% purity) and Cr target (2-inch diameter and 5-mm thickness; 99.99% purity) was placed in DC-powered sputtering guns placed at 120° apart from each other at the bottom of the chamber. Si substrates were initially cleaned with acetone and then dried in the air before clamping to the substrate holder. The substrate holder was rotated at a speed of 10 rpm to ensure the homogeneous deposition of the film over the substrates. The sputtering chamber was evacuated at a base pressure of 3×10^{-6} mbar in order to eliminate the impurities and contaminants. Argon (99.999% purity) as a processed gas (30 sccm) was inserted in the chamber, and the pressure during sputter deposition was kept constant at 3×10^{-2} mbar during deposition. DC power of 250 W was supplied to the Ni_3Al target to deposit Ni_3Al film (namely, 0 W Cr). To vary the concentration of Cr in Ni_3Al films, the power supply to Cr target was varied from 10 W to 40 W in steps of 10 W to deposit Cr-Ni_3Al alloy films, namely, 10 W Cr; 20 W Cr; 30 W Cr and 40 W Cr. Prior to deposition, pre-sputtering of 5 minutes was done on both the targets to remove the impurity from the surface of the targets whereas the actual sputtering was done for a duration of 1 hour. Other than the DC power to the Cr target, all the sputtering parameters were kept constant during all depositions.

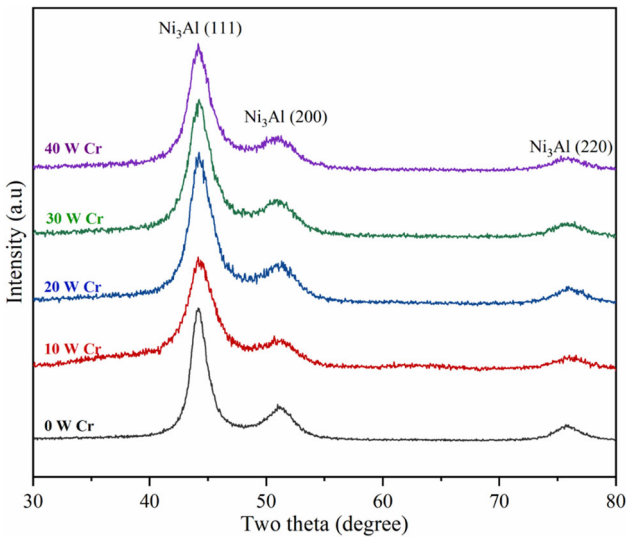

Fig. 1 GIXRD spectra of Ni_3Al and Cr-Ni_3Al alloy films

2.2 Characterization of Phase and Microstructure

Grazing angle x-ray diffraction (Empyrean PANalytical) was used to detect the phases of Ni_3Al-based films using CuKα = 0.154 Å at ambient temperature. The microstructure and surface topography of the films were characterized by FE-SEM (Zeiss Gemini) and atomic force microscopy (NaioAFM, Nanosurf, Switzerland). The elemental composition of Cr in Ni_3Al films was characterized using energy-dispersive spectroscopy equipped with FE-SEM.

2.3 Nanoindentation and Contact Angle Measurements

Quasi-static nanoindentation (nano-DMA, Hysitron Inc., Minneapolis, USA, TI-900) was performed to investigate the hardness and Young's modulus of Ni_3Al and Cr-Ni_3Al coatings. The depth-control nanoindentation test was performed at ambient temperature with a strain rate of 0.05^{-1} calibrated at a Poisson's ratio of 0.25. The average depth of penetration during the nanoindentation test was 100 nm and kept constant throughout the set of experiments. The mechanical property in terms of hardness and Young's modulus was calculated using Oliver and Pharr's technique by the inbuilt software in the nanoindentation setup. A total of 20 indents were made using a Berkovich diamond tip to calculate the average value of hardness and Young's modulus.

In order to measure the contact angle to study the hydrophobic properties of the films, a drop shape analysis experiment (DSA 100, Krüss GmbH, Germany) was performed. Distilled water droplets of 0.5 μl were dropped on 10 different places of the deposited surface in order to calculate the average contact angle between the deposited surface and water droplets. The contact angle and the profile of the water droplets dropped over the deposited surface were calculated using the camera and backlight installed in the setup. The experiment was conducted at ambient temperature in static conditions.

3. Results and Discussion

3.1 Identification of Phase and Microstructure

XRD patterns of Cr-Ni_3Al alloy coatings with different concentrations of Cr in alloy form are shown in Fig. 1. It can be seen that the Ni_3Al film (0 W Cr) displays a preferred (111) orientation at 44.13° followed by low-intensity diffraction peaks of (200) and (220) planes at 51.3° and 75.2° of face-centered cubic structure, respectively (Ref 27-29). These diffraction peaks are also in accord with the standard intermetallic $L1_2$ diffraction peaks of Ni_3Al. XRD patterns of Cr-Ni_3Al films do not display any evidential diffraction peaks of Cr. This is attributed to the substitution of Ni by Cr atoms from the host Ni_3Al lattice structure which causes the strain to induce in the film (Ref 22, 26). When Cr replaces Ni atoms of the host Ni_3Al lattice structure, it causes the formation of tensile residual stress. The value of strain in Ni_3Al and Cr-Ni_3Al calculated from the prominent peak of XRD spectra using Eq 1 (Ref 30) is shown in Table1.

$$\epsilon = \beta/4 \tan\theta \qquad \text{(Eq 1)}$$

where ε is microstrain, β is FWHM and θ is Bragg's angle.

The microstructure of Cr-Ni_3Al is characterized using FE-SEM as shown in Fig. 2. From the figure, it is seen that 0 W Cr-

Table 1 Calculated parameters of Cr-Ni_3Al coatings as a function of Cr enrichment

SN	Sample	Cr, at.%	Grain size, nm	Surface roughness, nm	Contact angle, degree	Porosity, %	Strain
1.	0 W Cr	0.00	91 ± 2.5	7.50 ± 0.23	75.5 ± 1.0	10.34	0.0195
2.	10 W Cr	1.07	110 ± 2.5	9.42 ± 0.27	98.4 ± 1.0	11.50	0.0213
3.	20 W Cr	2.25	139 ± 4.0	11.91 ± 0.42	111.9 ± 1.0	11.69	0.0229
4.	30 W Cr	5.71	166 ± 5.0	12.63 ± 0.63	112.5 ± 1.0	12.52	0.0244
5.	40 W Cr	7.34	195 ± 5.0	14.80 ± 0.71	115.9 ± 1.5	14.05	0.0269

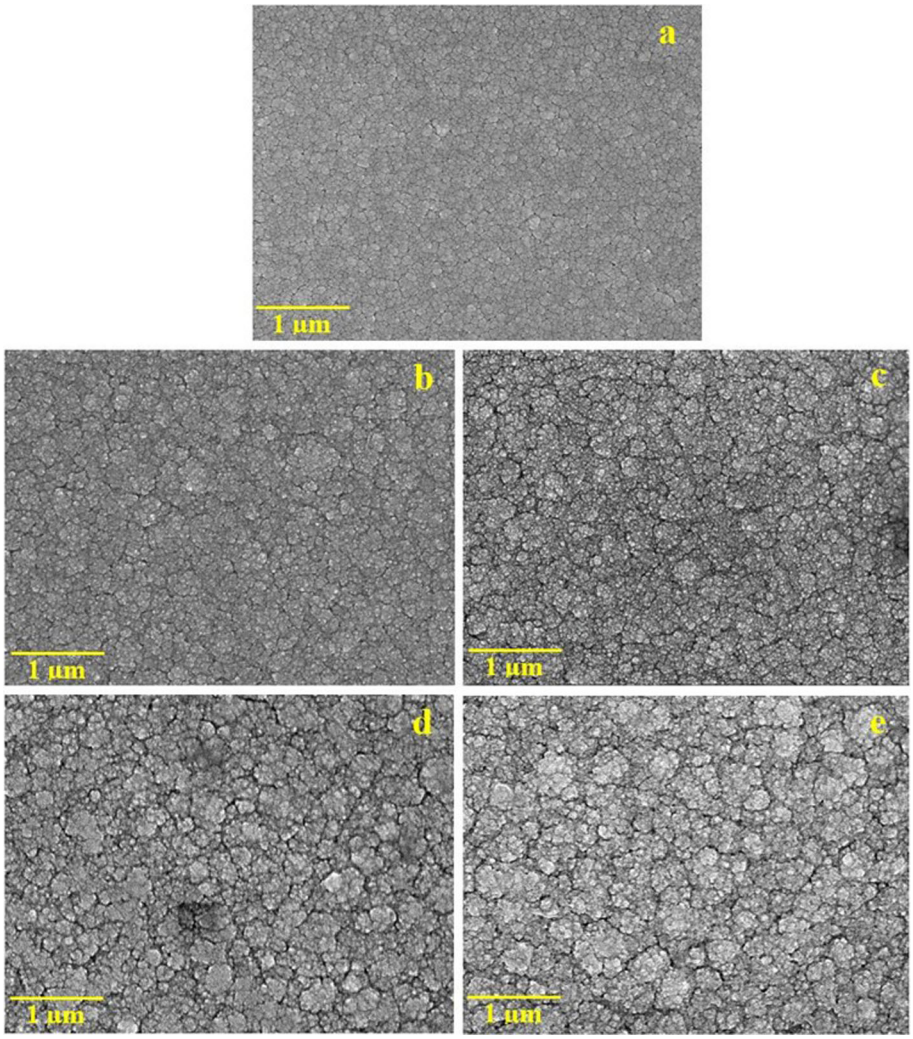

Fig. 2 FE-SEM images of Cr-Ni_3Al films (a) 0 W Cr, (b) 10 W Cr, (c) 20 W Cr, (d) 30 W Cr and (e) 40 W Cr

Ni_3Al film exhibits fine, equisized and densely packed consolidated grains reflecting smooth and homogeneous microstructure. Furthermore, in 10 W Cr-Ni_3Al film, there is the evolution of coarser grains and pores on the morphology of the deposited film resulting in inhomogeneous microstructure. A simultaneous increase in microcracks and pores is observed with a further increase in the Cr content (up to 40 W Cr) in the host Ni_3Al film. This could be the result of the agglomeration of crystallites resulting in grain growth which later contributes to deteriorating the arrangements of grains and grain boundaries. ImageJ software is used to calculate the percentage of porosity in the film using the SEM images of the Cr-Ni_3Al films (Ref 31). Results revealed that 0 W Cr-Ni_3Al films exhibited minimum percentage of pores (10.3%) whereas 40 W Cr-Ni_3Al films showed the maximum percentage of pores (14%) in the film as shown in Table 1.

Furthermore, the grain size of the deposited films has also been calculated using ImageJ software. For this purpose, we have used the FE-SEM images. The distribution of grain size in Ni_3Al and Cr-Ni_3Al films is shown in Fig. 3. From the figure, it

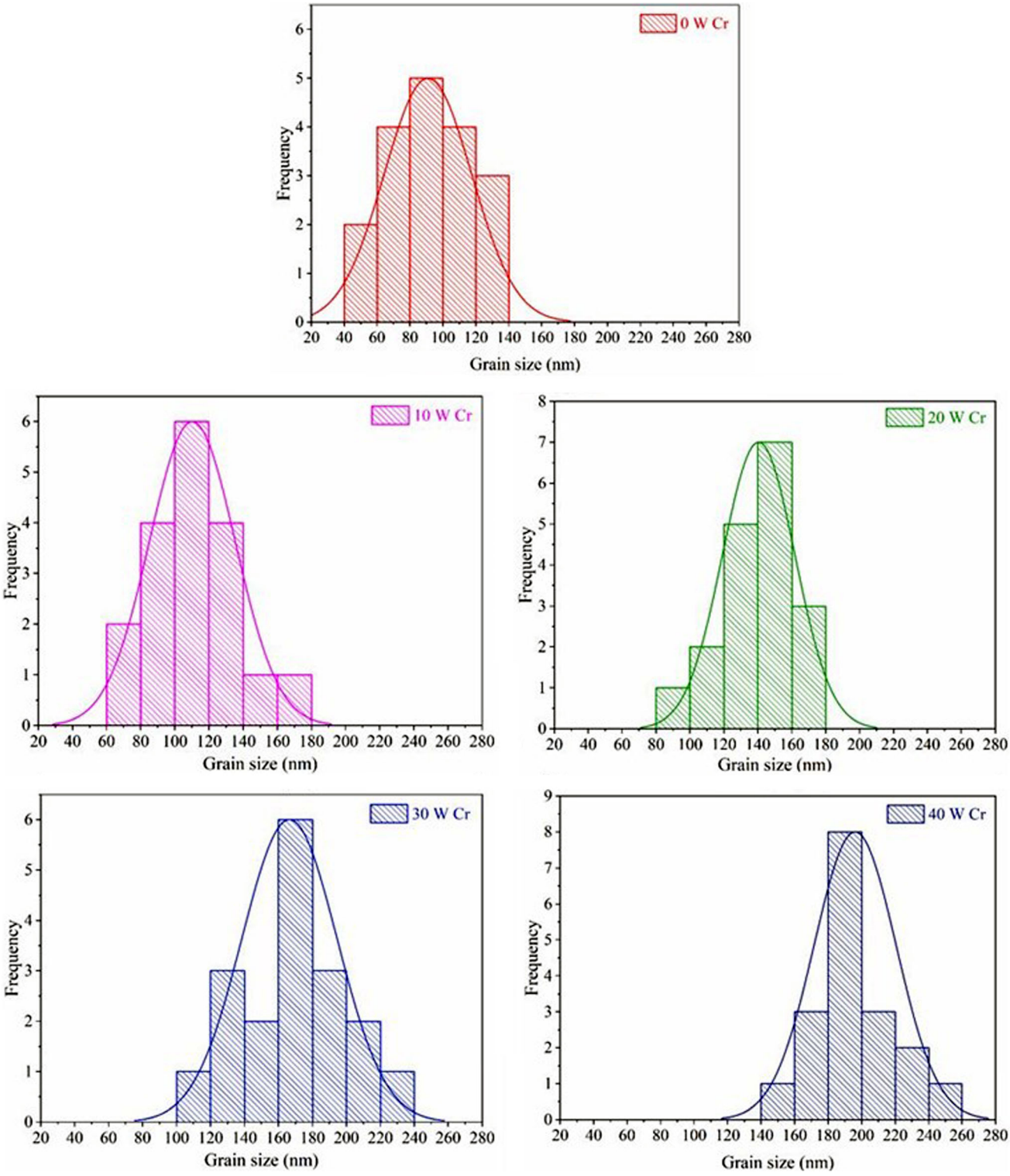

Fig. 3 Distribution of grains in Cr-Ni_3Al coatings

is observed that 10 W Cr-Ni_3Al reflects the homogeneous distribution of smaller grains with an average grain size of 91 ± 2.5 nm. With further increase in Cr content in the film, the distribution of grains becomes inhomogeneous as a result of grain coarsening which simultaneously continues up to 40 W Cr enrichment in the film. The minimum and maximum grain size of 91 ± 2.5 and 195 ± 5.0 nm have been calculated for 10 W Cr-Ni_3Al and 40 W Cr-Ni_3Al film, respectively (Ref 31).

The surface topography of deposited alloy films has been studied and explored using atomic force microscopy. The cantilever probe of AFM scanned an area of 10 × 10 μm^2 to reveal information about the surface asperities of the deposited

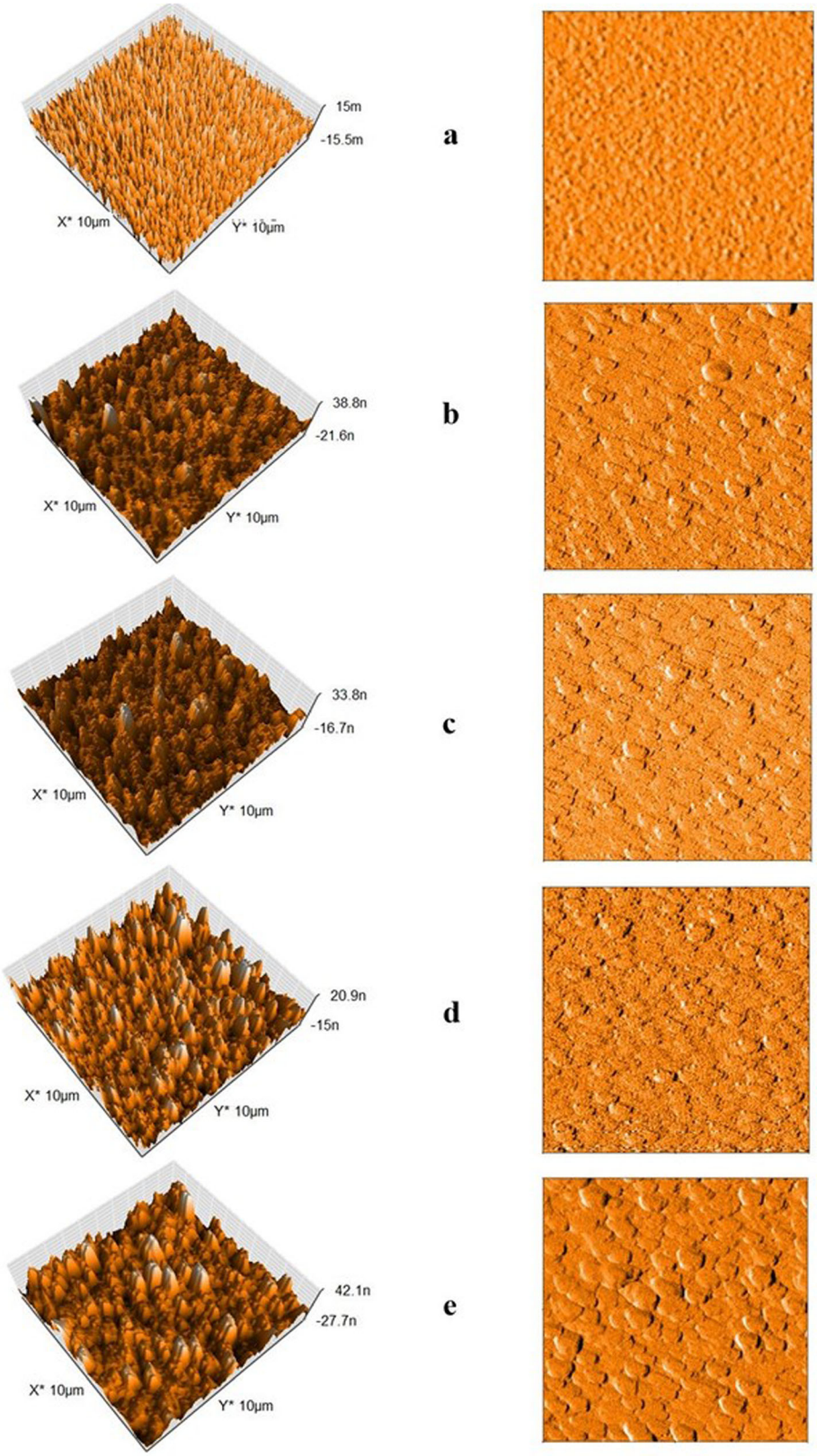

Fig. 4 Three-dimensional and 2D AFM images of Cr-Ni_3Al films (a) 0 W Cr, (b) 10 W Cr, (c) 20 W Cr, (d) 30 W Cr and (e) 40 W Cr

films. However, to calculate the average surface roughness (rms) of the film, the area of 50 × 50 μm^2 was scanned at 10 different spots. Figure 4 shows the 2D and 3D AFM images of Cr-Ni_3Al films. From the figure, it can be observed that the Ni_3Al film with 0 W Cr exhibits closely packed high frequency of fine, thin and sharp hill-type structured nano-asperities of less intensity. A subsequent and continuous increase in a dome-like broad asperities with distorted structures has been observed

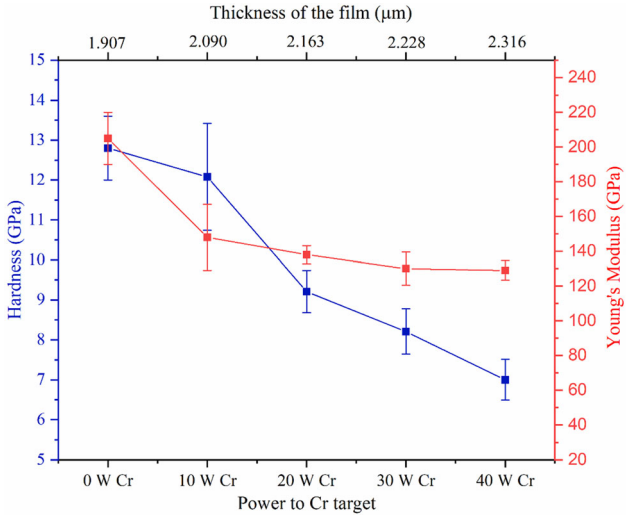

Fig. 5 Hardness and Young's modulus of Cr-Ni_3Al films as a function of power to Cr target

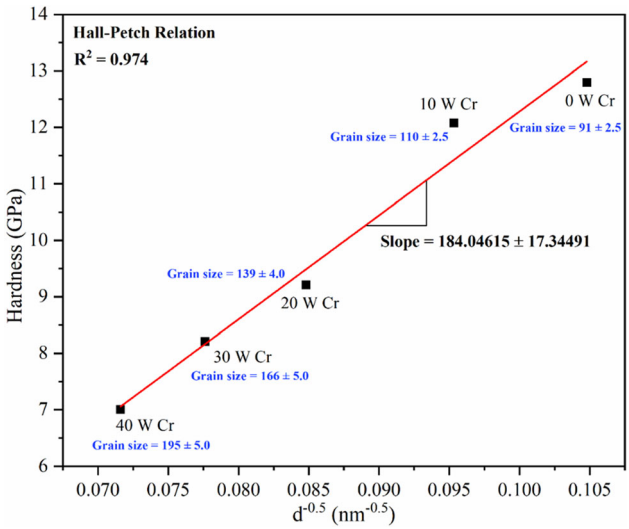

Fig. 6 Hall–Petch relationship of Ni_3Al and Cr-Ni_3Al films

in Cr-Ni_3Al coatings as a result of increase in Cr content. This led to an increase in surface roughness and also an increase in void fraction. The surface roughness (rms) of the deposited films calculated using AFM is reported in Table 1. The minimum and maximum surface roughness of 7.50 ± 0.23 nm and 14.80 ± 0.71 nm have been observed for 0 W Cr-Ni_3Al and 40 W Cr-Ni_3Al films, respectively.

3.2 Contact Angle Measurements

Contact angle measurements have been performed and examined on a drop shape analyzer at ambient temperature. In order to study the hydrophobic property of the film, the contact angle has been measured between water droplets and the deposited surface with different concentrations of Cr in steady state as shown in Table 1. Results showed that the contact angle increases simultaneously with increase in Cr concentration in Ni_3Al film. This could be the result of the subsequent increase in the surface roughness of the film with Cr enrichment as indexed in Table 1. With the increase in surface roughness of

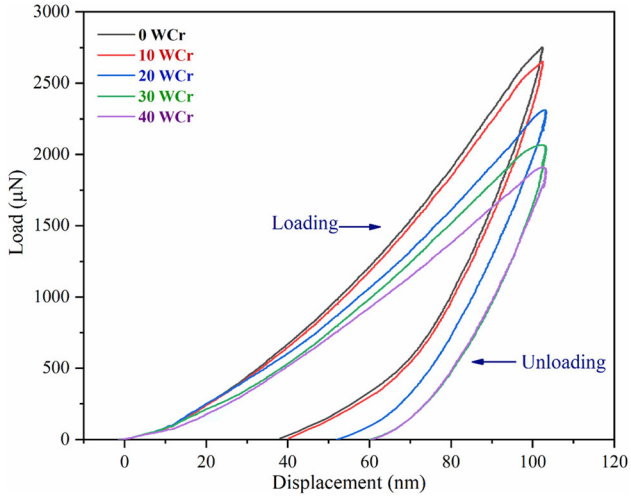

Fig. 7 Load versus displacement graph of Cr-Ni_3Al films

the film, there is increase in void fraction too. These available voids between the nano-asperities of the surface help in trapping the air which decreases the surface contact area between water and deposited films and thus increases the hydrophobic property of the film (wettability is decreased). It has been reported in the literature that increase in surface roughness increases the hydrophobic property of the film up to a limit (Ref 28). From the results of AFM, it can be seen that there is a sudden increase in surface roughness of 10 W Cr-Ni_3Al films (7.50 nm-9.42 nm) which lead to a dramatic rise in water contact angle too. However, the marginal difference in surface roughness of 20 W Cr-Ni_3Al and 30 W Cr-Ni_3Al (11.91 nm-12.63 nm) has reflected a small degree of variation in contact angle. The lowest and highest contact angle of 75.5° and 115.9° have been found for 0 W Cr-Ni_3Al and 40 W Cr-Ni_3Al coatings, respectively. The work shows the efficient method to deposit the Ni_3Al films with Cr enrichment which convert the hydrophilic films to hydrophobic in nature for their application in microelectronic devices which facilitates heat dissipation.

3.3 Mechanical Properties

Mechanical properties of Cr-Ni_3Al have been investigated in terms of nano-hardness and Young's modulus. Depth-control quasi-static nanoindentation was used to evaluate the results of mechanical properties at ambient temperature. The results of nano-hardness and Young's modulus are plotted in Fig. 5. It can be observed that the hardness of the film decreased with increase in power supply to Cr target. This is because of the increase in Cr content in host Ni_3Al film (as a result of the increase in power supply to Cr target) which led to an increase in the overall film thickness which further contributes to agglomeration of crystallites resulting in grain size enlargement. Furthermore, the larger grains contributed to the generation of large volumes of microcracks and pores (Table 1) which led to the degradation of the microstructure of the film. Figure 6 shows the summarized result of hardness versus inverse square root of the grain size. From the figure, it can be observed that the hardness of the film is directly proportional to the inverse square root of grain size obeying the classical Hall–Petch relation. This is evident that the hardness of the film decreases with increase in grain size following the dislocation

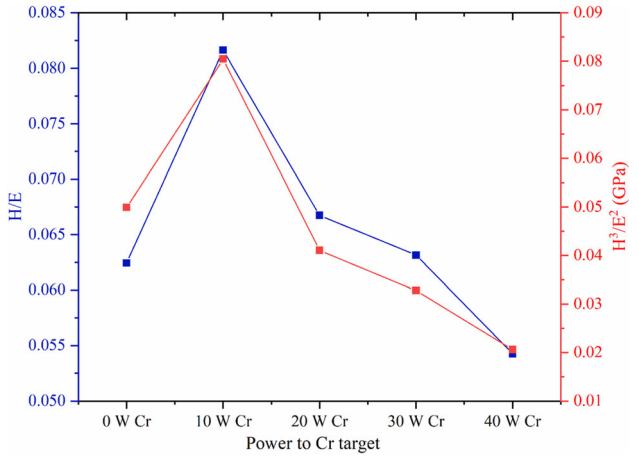

Fig. 8 H/E and H^3/E^2 ratios of Ni_3Al coatings enriched with Cr content

pileup model. The films with smaller grain sizes consisted of large volumes of grain boundaries which resist the dislocation movement across the boundaries and are piled up near the grain boundaries which led to the enhancement in hardness (Ref 30, 32). Moreover, the value of R^2 is very close to 1 ($R^2 = 0.974$) which suggests that the regression line fits the data well resulting in a high value of H–P coefficient [slope = 184.04615 ± 17.34491 GPa ($nm^{1/2}$)]. The literature shows that the H–P coefficient of the nanomaterials is in the range of 40-144 with hardness in the range of 10 GPa-17 GPa (Ref 33-35). It is also reported that the hardness of the film increases with increase in H–P coefficient. In our case, however, the value of the H–P coefficient is higher, but the presence of cracks and pores in the films degrades the microstructure resulting in the evolution of hardness in the range of ~ 7-12.7 GPa.

It has also been reported that the variation in hardness as a function of grain size is compensated by the chemical ordering of FCC Ni_3Al film (formation of thermodynamic equilibrium Ni_3Al $L1_2$ phase) (Ref 25) which says that with the increase in grain size, the hardness of the film increases if the ordered equilibrium $L1_2$ Ni_3Al phase is formed in nanocrystalline films (Ref 23, 25, 36). In our case, the XRD spectrum of Ni_3Al film (0 W Cr) showed a prominent peak of Ni_3Al (111) at 44.13° which is also in accord with the standard intermetallic $L1_2$ structure contributing in increasing the hardness of the film. However, the presence of the pores in Cr-Ni_3Al films contributes in lowering the hardness of the alloy Cr-Ni_3Al films. The evolution in Young's modulus also shows the same trend as reflected by the nano-hardness curve. Figure 7 reflects the load versus depth curve as a function of Cr enrichment in Ni_3Al alloy films. A maximum load (P_{max}) of 2.8 mN is recorded during depth-control nanoindentations. From the figure, it can be observed that the deposited films showed both elastic and plastic deformations during loading whereas only elastic deformation has been observed during unloading (Ref 35). Moreover, 0 W and 10 W Cr-Ni_3Al samples reflected almost the same permanent deformation depth of ~ 38 nm and ~ 40 nm, respectively, whereas 20 W Cr-Ni_3Al samples showed a permanent deformation depth of ~ 46 nm. The maximum permanent deformation depth of 60 nm is observed for both 30 W Cr-Ni_3Al and 40 W Cr-Ni_3Al films. This shows that 0 W Cr and 10 W Cr possess a better rate of elastic recovery as compared to 20 W Cr, 30 W Cr and 40 W Cr films. The highest value of H/E and H^3/E^2 calculated from the results of nanoindentation (Fig. 8) is evident that 10 W Cr-Ni_3Al film imitates better resistance to plastic deformation whereas the 40 W Cr-Ni_3Al reflects the maximum plastic deformation. This also reveals that the toughness of the Ni_3Al coatings decreased with increase in Cr concentration (Ref 35, 37, 38). Xing et al. (2013) (Ref 26) also found similar results in terms of a decrease in hardness when they synthesized Cr/Ni_3Al multilayer films. It has been reported that the Ni_3Al films in multilayer forms when enriched with nickel have reflected a hardness in the range of ~ 4.5-8 GPa (Ref 24, 39-41). Some studies based on doped Ni_3Al with transition metals in multilayer forms followed by heat treatment have shown an increase in the hardness beyond 8 GPa (Ref 19, 23, 25). Researchers have found that the hardness of Ni_3Al-based multilayer thin films is mostly influenced by the microstructure, layer thickness, indentation depth and annealing at high temperatures (Ref 42, 43). However, very limited research has been reported in the literature on the case of doped Ni_3Al films in alloy forms. In our case, the maximum and minimum hardness of 12.7 ± 0.8 GPa and 7.0 ± 0.5 GPa have been observed for 0 W Cr-Ni_3Al and 40 W Cr-Ni_3Al alloy films whereas the maximum and minimum Young's modulus of 203 ± 15 GPa and 129 ± 5.6 GPa have been observed for 0 W Cr-Ni_3Al and 40 W Cr-Ni_3Al, respectively. The Ni_3Al-based coatings with high hardness reported in this work can be used in scratch-resistant connectors, slider and other components of electronic devices and molding dies.

4. Conclusion

Ni_3Al and Cr-Ni_3Al alloy films with variations in Cr concentration have been synthesized via DC magnetron sputtering. The microstructure, phase and mechanical properties of the deposited films have been investigated. XRD patterns of Ni_3Al and Cr-Ni_3Al alloy films have reflected a preferred orientation of the (111) plane followed by low-intensity peak of (200) and (220). However, no evidence of Cr in diffraction peak of Cr-Ni_3Al films has been observed upon enriching the host Ni_3Al film with Cr. The increase in sputtering power to the Cr target resulted in enriching the Cr content in the films which further led to the evolution of porosity resulting in degradation of the surface roughness. The maximum percentage of pores (14%) have been observed in 40 W Cr-Ni_3Al films with highest surface roughness of 14.80 ± 0.71 nm. 0 W Cr-Ni_3Al alloy film has shown the highest value of hardness (12.7 ± 0.8 GPa) and Young's modulus (203 ± 15 GPa) that decrease with increase in Cr content. Contact angle measurements reveal that Cr-Ni_3Al films are hydrophilic in nature but converts to hydrophobic with increase in Cr content in the samples. The maximum contact angle of 115.9° is observed for 40 W Cr-Ni_3Al films.

Acknowledgment

The authors would like to express their sincere gratitude to the Central Instrumentation Center (CIC) at the University of Petroleum and Energy Studies (UPES) for support in synthesis and characterization.

References

1. K. Gong, H. Luo, D. Feng, and C. Li, Wear of Ni_3Al-Based Materials and Its Chromium-Carbide Reinforced Composites, *Wear*, 2008, **265**(11–12), p 1751–1755
2. D. Lee, An Investigation of Thermal Aging Effects on the Mechanical Properties of a Ni_3Al-Based Alloy by Nanoindentation, *J. Alloys Compd.*, 2009, **480**(2), p 347–350
3. S. Zhu, Q. Bi, J. Yang, W. Liu, and Q. Xue, Influence of Cr Content on Tribological Properties of Ni_3Al Matrix High Temperature Self-Lubricating Composites, *Tribol. Int.*, 2011, **44**(4), p 445–53. https://doi.org/10.1016/j.triboint.2011.05.014
4. S. Kang and J.H. Selverian, Effect of Active Metal Coatings on the Mechanical Properties of Silicon Nitride-Based Ceramics, *J. Mater. Sci.*, 1993, **28**(20), p 5514–5520. https://doi.org/10.1007/BF00367823
5. J.W. Du, L. Chen, J. Chen, and Y. Du, Mechanical Properties Thermal Stability and Oxidation Resistance of TiN/CrN Multilayer Coatings, *Vacuum*, 2020, **179**, p 109468. https://doi.org/10.1016/j.vacuum.2020.109468
6. M. Diserens, J. Patscheider, and F. Lévy, Mechanical Properties and Oxidation Resistance of Nanocomposite TiN-SiNx Physical-Vapor-Deposited Thin Films, *Surf. Coat. Technol.*, 1999, **120–121**, p 158–165
7. W.J. Tomlinson and G.R. Wilson, The Oxidation of Electroless Ni-B and Ni-P Coatings in Air at 800 to 1000 °C, *J. Mater. Sci.*, 1986, **21**(1), p 97–102
8. H.P. Ng, X.K. Meng, and A.H.W. Ngan, An Investigation into the Fabrication and Properties of Ni_3Al Thin Coatings on Nickel Substrates, *Scr. Mater.*, 1998, **39**(12), p 1737–1742
9. N. Li, M. Wang, G. Zheng, Y. Li, and G. Chen, Composition Distribution and Electrochemical Behavior of an Ni_2Al_3 Coating on Q235 Steel, *Metals*, 2016, **6**(3), p 17–23
10. S.K. Tiwari, A.U. Rao, A.S. Kharb, A.K. Chawla, and D.K. Avasthi, A Review of Mechanical and Tribological Properties of Ni_3Al-Based Coatings-Synthesis and High-Temperature Behavior, *Phys. Scr.*, 2023, **98**(7), p 72001. https://doi.org/10.1088/1402-4896/acd81c
11. A.U. Rao, S.K. Tiwari, M.S. Goyat, and A.K. Chawla, Recent Developments in Magnetron-Sputtered Silicon Nitride Coatings of Improved Mechanical and Tribological Properties for Extreme Situations, *J. Mater. Sci.*, 2023, **58**(24), p 9755–9804. https://doi.org/10.1007/s10853-023-08575-4
12. J. Duszczyk, J. Zhou, L. Marvina, and L.Z. Zhuang, In-Situ Reactive Synthesis of the Ni_3Al Intermetallic Compound and Subsequent Diffusion Bonding with Different Steels for Surface Coating, *J. Mater. Sci.*, 1999, **34**(16), p 3937–3950
13. C. Sun, S.A. Maloy, K. Baldwin, Y. Wang, and J.A. Valdez, Phase Stability of Ni/Ni3Al Multilayers Under Thermal Annealing and Irradiation, *Jom*, 2020, **72**(11), p 3995–4001
14. D. Kourtidou, D. Chaliampalias, C. Vogiatzis, E. Tarani, A. Kamou, E. Pavlidou, S. Skolianos, K. Chrissafis, and G. Vourlias, Deposition of Ni-Al Coatings by Pack Cementation and Corrosion Resistance in High Temperature and Marine Environments, *Corros. Sci.*, 2019, **148**, p 12–23. https://doi.org/10.1016/j.corsci.2018.11.003
15. S.A. Serna, J.A. Verduzco, B.F. Campillo, A. Molina, R. Guardian, A. del Pozo, A. Sedano, and H. Villanueva, Synthesis and Characterization of a Ni_3Al Intermetallic Modified with Copper Atoms via Powder Metallurgy, *J. Mater. Eng. Perform*, 2021, **30**(3), p 1906–1913. https://doi.org/10.1007/s11665-021-05541-6
16. C. Yan, Y. Kang, L. Kong, and S. Zhu, Tribological Properties of Ni_3Al Matrix Composite Sliding Against Si_3N_4, SiC and Al_2O_3 at Elevated Temperatures, *J. Mater. Eng. Perform.*, 2017, **26**(1), p 168–176
17. T. Chandanayaka and F. Azarmi, Investigation on the Effect of Reinforcement Particle Size on the Mechanical Properties of the Cold Sprayed Ni-Ni_3Al Composites, *J. Mater. Eng. Perform.*, 2014, **23**(5), p 1815–1822
18. A.N. Filippin, T.Y. Lin, M. Rawlence, T. Zünd, K. Kravchyk, J. Sastre-Pellicer, S.G. Haass, A. Wäckerlin, M.V. Kovalenko, and S. Buecheler, Ni-Al-Cr Superalloy as High Temperature Cathode Current Collector for Advanced Thin Film Li Batteries, *RSC Adv.*, 2018, **8**(36), p 20304–20313
19. C. Zhang, K. Feng, Z. Li, F. Lu, J. Huang, Y. Wu, and P.K. Chu, Enhancement of Hardness and Thermal Stability of W-Doped Ni_3Al Thin Films at Elevated Temperature, *Mater. Des.*, 2016, **111**, p 575–583
20. M. Nastasi, L.S. Hung, and J.W. Mayer, Phase Formation by Ion Beam Mixing in Ni/Al, Pd/Al, and Pt/Al Bilayers, *Appl. Phys. Lett.*, 1983, **43**(9), p 831–833
21. I. Stloukal, J. Čermák, J. Růžičková, and A. Pokorná, Iron Grain Boundary Diffusion in Pure and in Cr, Fe and Zr-Doped Ni_3Al Alloys, *Intermetallics*, 1999, **7**(1), p 33–38
22. K. Aoki, K. Ishikawa, and T. Masumoto, Ductilization of Ni_3Al by Alloying with Boron and Substitutional Elements, *Mater. Sci. Eng. A*, 1995, **192–193**(Part 1), p 316–323
23. C. Zhang, K. Feng, Z. Li, F. Lu, J. Huang, and Y. Wu, Microstructure and Mechanical Properties of Sputter Deposited Ni/Ni_3Al Multilayer Films at Elevated Temperature, *Appl. Surf. Sci*, 2016, **378**, p 408–417. https://doi.org/10.1016/j.apsusc.2016.04.027
24. C.-C. Wu and F.-B. Wu, Microstructure and Mechanical Properties of Magnetron Co-Sputtered Ni-Al Coatings, *Surf. Coat. Technol.*, 2009, **204**(6–7), p 854–859
25. R. Banerjee, Hardness of Sputter Deposited Nanocrystalline Ni_3Al Thin Films, *Mater. Lett.*, 2007, **61**(2), p 609–612
26. Y.Y. Xing, B. Dai, X.H. Wei, Y.J. Ma, and M. Wang, Enhancement of High-Temperature Oxidation Resistance and Mechanical Properties of Ni3Al Thin Films by Inserting Ultrathin Cr Layers, *Vacuum*, 2014, **101**, p 107–112
27. H. Van Swygenhoven, P. Bijni, F.T. Division, and C. Villigen, *Nanostruct. N Al Produced Sputtering Magn.*, 1995, **6**(95), p 3
28. S.K. Tiwari, A.U. Rao, V. Chawla, P. Dubey, V. Saxena, A.K. Chawla, and D.K. Avasthi, Synthesis and Characterization of Sputter-Deposited Ni-Rich Ni_3Al Hard Coatings, *J. Alloys Compd.*, 2022, **926**, p 166802. https://doi.org/10.1016/j.jallcom.2022.166802
29. C. Zhang, K. Feng, Z. Li, F. Lu, J. Huang, and Y. Wu, Applied Surface Science Microstructure and Mechanical Properties of Sputter Deposited Ni/Ni_3Al Multilayer Films at Elevated Temperature, *Appl. Surf. Sci.*, 2016, **378**, p 408–417. https://doi.org/10.1016/j.apsusc.2016.04.027
30. B. Heryanto and D. Abdullah, Quantitative Analysis of x-Ray Diffraction Spectra for Determine Structural Properties and Deformation Energy of Al, Cu and Si, *J. Phys. Conf. Ser.*, 2019, **1317**(1), p 12052
31. N.H. Astuti, N.A. Wibowo, and M.R. Ayub, The Porosity Calculation of Various Types of Paper Using Image Analysis, *J. Pendidik. Fis. Indones.*, 2018, **14**(1), p 46–51
32. R. Wang, J. Deng, Z. Zhang, and D. Ge, Microstructure and Tribological Properties of Ni_3Al Matrix Micro-Laminated Films Deposited by Electrohydrodynamic Atomization, *Appl. Surf. Sci.*, 2022, **606**(September), p 154918. https://doi.org/10.1016/j.apsusc.2022.154918
33. J.A. Wollmershauser, B.N. Feigelson, E.P. Gorzkowski, C.T. Ellis, R. Goswami, S.B. Qadri, J.G. Tischler, F.J. Kub, and R.K. Everett, An Extended Hardness Limit in Bulk Nanoceramics, *Acta Mater.*, 2018, **2014**(69), p 9–16. https://doi.org/10.1016/j.actamat.2014.01.030
34. R. Banerjee, G. Thompson, P. Anderson and H. Fraser, Sputter Deposited Nanocrystalline Ni-25Al Alloy Thin Films and Ni/Ni_3Al Multilayers, *Thin Solid Films*, 2003, **424**(1), p 93–98. https://doi.org/10.1016/S0040-6090(02)00924-0
35. N. Li, M. Wang, G. Zheng, P. Li, Y. Li, and G. Chen, Ni_2Al_3 Intermetallic Coating: Microstructure and Mechanical Properties, *Adv. Mater. Process. Technol.*, 2018, **4**(2), p 255–261. https://doi.org/10.1080/2374068X.2017.1414996
36. R.L. Doiphode, S.V.S.N. Murty, N. Prabhu, and B.P. Kashyap, Grain Growth in Calibre Rolled Mg-3Al-1Zn Alloy and Its Effect on Hardness, *J. Magnes. Alloy*, 2015, **3**(4), p 322–329. https://doi.org/10.1016/j.jma.2015.11.003
37. D. Yang, H. Chen, Y. Ye, C. Wang, H. Zhao, and D. Gong, Doping Silicon to Enhance the Anti-Corrosion and Anti-Wear Abilities of Chromium Nitride Coating in Seawater, *Surf. Topogr. Metrol. Prop.*, 2018, **6**(4), p 044001. https://doi.org/10.1088/2051-672X/aaee9e
38. L.-C. Chang, M.-C. Sung, and Y.-I. Chen, Effects of Bias Voltage and Substrate Temperature on the Mechanical Properties and Oxidation Behavior of CrSiN Films, *Vacuum*, 2021, **194**, p 110580. https://doi.org/10.1016/j.vacuum.2021.110580
39. X. Chen, Y. Du, and Y. Chung, Commentary on Using H/E and H^3/E^2 as Proxies for Fracture Toughness of Hard Coatings, *Thin Solid Films*, 2019, **688**(April), p 137265. https://doi.org/10.1016/j.tsf.2019.04.040
40. X.K. Meng, H. Vehoff, and A.H.W. Ngan, Hard Multilayered Thin Films of Metal-Intermetallic Ni/Ni_3Al, *J. Mater. Res.*, 2000, **15**(12), p 2595–2597. https://doi.org/10.1557/JMR.2000.0371

41. S. Tixier, P. Böni, and H. Van Swygenhoven, Hardness Enhancement of Sputtered Ni_3 Al/Ni Multilayers, *Thin Solid Films*, 1999, **342**(1–2), p 188–193
42. X.K. Meng, H. Shen, H. Vehoff, S. Mathur, and A.H.W. Ngan, Fractography, Elastic Modulus, and Oxidation Resistance of Novel Metal-Intermetallic Ni/Ni_3Al Multilayer Films, *J. Mater. Res.*, 2002, **17**(4), p 790–796. http://hdl.handle.net/10722/42408
43. S.K. Tiwari, A.U. Rao, A.S. Kharb, V. Chawla, N. Sardana, D.K. Avasthi, and A.K. Chawla, Investigation of Mechanical and Microstructural Properties of Sputter-Deposited Zr-Ni_3Al Coatings, *J. Vac. Sci. Technol. A,* 2023, **41**(6), p 063407